Published online 12 October 2020 *Nucleic Acids Research, 2020, Vol. 48, No. 19* ***11113–11129***
doi: 10.1093/nar/gkaa860

Asymmetrical effects of deafness-associated mitochondrial DNA 7516delA mutation on the processing of RNAs in the H-strand and L-strand polycistronic transcripts

Yun Xiao[1,2,3,†], Meng Wang[1,2,†], Qiufen He[1,2], Lei Xu[3], Qinghai Zhang[1,2], Feilong Meng[1,2], Zidong Jia[1], Fengguo Zhang[3], Haibo Wang[3,*] and Min-Xin Guan[1,2,4,5,*]

[1]Division of Medical Genetics and Genomics, The Children's Hospital, Zhejiang University School of Medicine and National Clinical Research Center for Child Health, Hangzhou, Zhejiang 310058, China, [2]Institute of Genetics, Zhejiang University School of Medicine, Hangzhou, Zhejiang 310058, China, [3]Department of Otolaryngology–Head and Neck Surgery, Shandong Provincial ENT Hospital, Shandong University, Jinan, Shandong 250022, China, [4]Key Lab of Reproductive Genetics, Ministry of Education of PRC, Zhejiang University, Hangzhou, Zhejiang 310058, China and [5]Joint Institute of Genetics and Genome Medicine between Zhejiang University and University of Toronto, Hangzhou, Zhejiang 310058, China

Received May 18, 2020; Revised September 10, 2020; Editorial Decision September 18, 2020; Accepted September 23, 2020

ABSTRACT

In this report, we investigated the molecular mechanism underlying a deafness-associated m.7516delA mutation affecting the 5′ end processing sites of mitochondrial tRNA^{Asp} and tRNA$^{Ser(UCN)}$. An *in vitro* processing experiment demonstrated that m.7516delA mutation caused the aberrant 5′ end processing of tRNA$^{Ser(UCN)}$ and tRNA^{Asp} precursors, catalyzed by RNase P. Using cytoplasmic hybrids (cybrids) derived from one hearing-impaired Chinese family bearing the m.7516delA mutation and control, we demonstrated the asymmetrical effects of m.7516delA mutation on the processing of tRNAs in the heavy (H)-strand and light (L)-strand polycistronic transcripts. Specially, the m.7516delA mutation caused the decreased levels of tRNA$^{Ser(UCN)}$ and downstream five tRNAs, including tRNA^{Tyr} from the L-strand transcripts and tRNA^{Asp} from the H-strand transcripts. Strikingly, mutant cybrids exhibited the lower level of COX2 mRNA and accumulation of longer and uncleaved precursors of COX2 from the H-strand transcripts. Aberrant RNA metabolisms yielded variable reductions in the mitochondrial proteins, especially marked reductions in the levels of ND4, ND5, CO1, CO2 and CO3. The impairment of mitochondrial translation caused the proteostasis stress and respiratory deficiency, diminished ATP production and membrane potential, increased production of reactive oxygen species and promoted apoptosis. Our findings provide new insights into the pathophysiology of deafness arising from mitochondrial tRNA processing defects.

INTRODUCTION

The mitochondrial RNA processing is essential for the formation of functional tRNAs used for mitochondrial translation (1–3). In humans, mitochondrial DNA (mtDNA) is circular and composed of two strands: heavy (H) strand encodes 2 rRNAs, 14 tRNAs and 12 polypeptides for essential subunits of the oxidative phosphorylation system (OXPHOS), and light (L) strand codes for 8 tRNAs and 1 polypeptide (ND6) (4,5). mtDNA bidirectionally produces the polycistronic H- and L-strand transcripts, catalyzed by the mitochondrial transcription machinery (6–10). As shown in Figure 1, the transcription of H-strand promoter 1 (HSP1) produces the short transcript containing 12S rRNA, 16S rRNA, tRNA^{Phe} and tRNA^{Val}, while the transcription initiated from HSP2 generates an almost genome transcript consisting of 12S rRNA, 16S rRNA, 12 mRNAs and 14 tRNAs, including tRNA^{Asp}, tRNA^{Lys} and tRNA$^{Leu(UUR)}$ (6,7,11,12). Furthermore, the transcription of L-strand promoter (LSP) resulted in a near-genomic length primary transcript encoding eight tRNAs, including tRNA^{Gln} and tRNA$^{Ser(UCN)}$, and ND6 (6,7,11,12). Af-

*To whom correspondence should be addressed. Tel: +86 571 88206916; Fax: +86 571 88206497; Email: gminxin88@zju.edu.cn
Correspondence may also be addressed to Haibo Wang. Tel: +86 531 68777588; Fax: +86 531 68777588; Email: whboto11@email.sdu.edu.cn
†The authors wish it to be known that, in their opinion, the first two authors should be regarded as Joint First Authors.

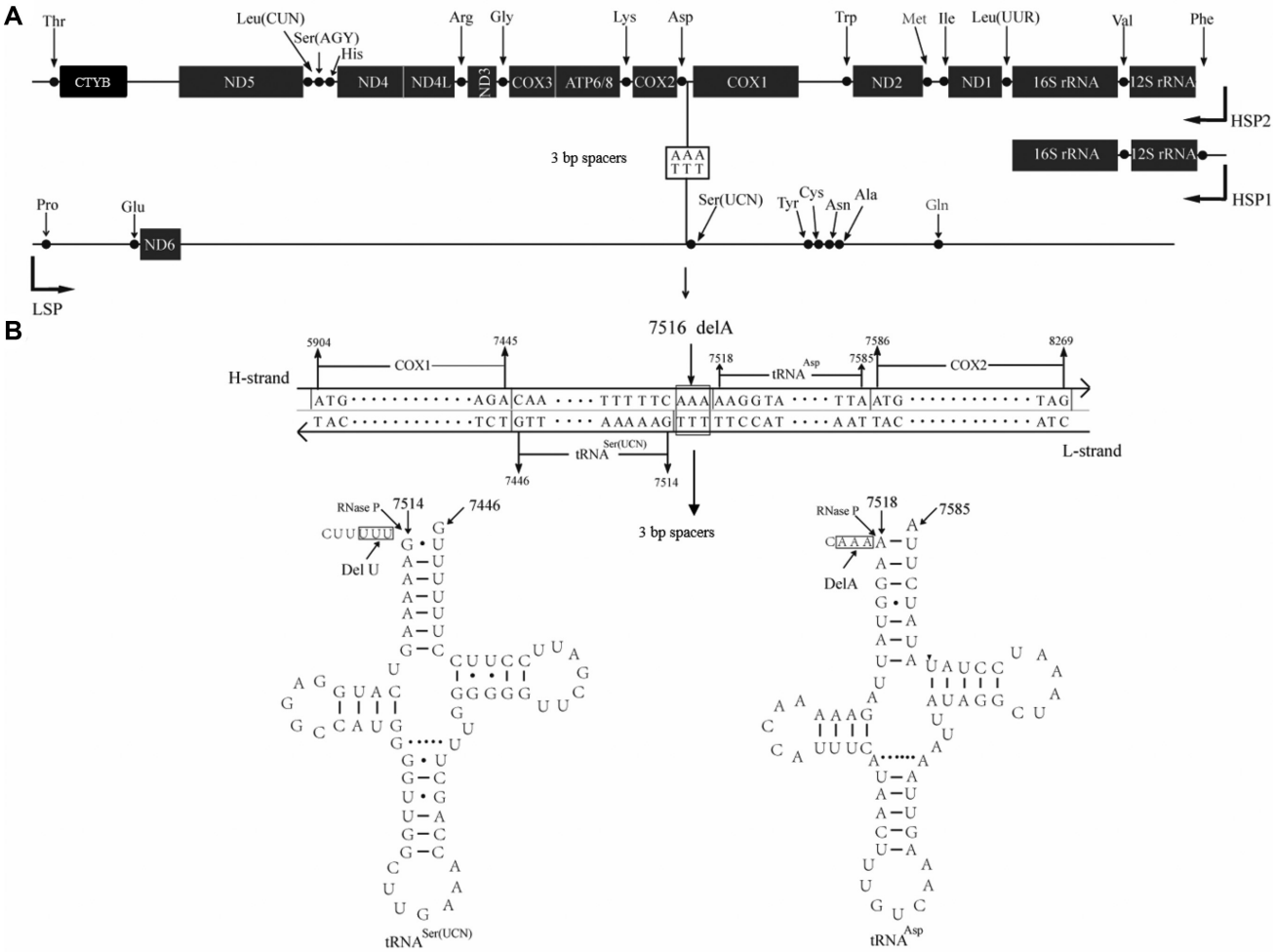

Figure 1. A schema of transcription map of human mitochondria and location of m.7516delA mutation in the precursors of $tRNA^{Ser(UCN)}$ and $tRNA^{Asp}$. (**A**) Three polycistronic RNA transcripts. The transcription of LSP resulted in a near-genomic length primary transcript encoding eight tRNAs and ND6. The transcription of HSP1 generated the short transcript containing $tRNA^{Phe}$, $tRNA^{Val}$, 12S rRNA and 16S rRNA, while the transcription from HSP2 produced an almost genome transcript consisting of 12S rRNA, 16S rRNA, 12 mRNAs and 14 tRNAs. (**B**) Location of m.7516delA mutation in the precursors of $tRNA^{Ser(UCN)}$ and $tRNA^{Asp}$. Cloverleaf structures of $tRNA^{Ser(UCN)}$ and $tRNA^{Asp}$ were derived from (28). Potential 5′ end processing sites in the $tRNA^{Ser(UCN)}$ and $tRNA^{Asp}$ precursors catalyzed by RNase P are indicated.

ter transcription, these polycistronic transcripts are processed to release 13 mRNAs, 22 tRNAs, and 2 rRNAs essential for mitochondrial translation (6,7). The processing of mitochondrial tRNAs from the primary transcripts required the precise cleavage of tRNAs at their 5′ ends, catalyzed by RNase P, and 3′ terminal mediated by RNase Z (13–16). In particular, the mRNA and rRNA at H-strand transcripts are flanked by one or more tRNAs, and the excision of tRNAs releases all other elements and is a prerequisite for RNA maturation. This processing mechanism was referred to as the tRNA punctuation model (7). However, the processing mechanisms of L-strand transcripts are different from those of H-strand transcripts, indicating the existence of complex posttranscriptional regulatory mechanisms (10,17). The aberrant 5′ or 3′ end processing of mitochondrial tRNA precursors has been linked to an array of different diseases, including deafness, cardiomyopathy and hypertension (18–26). The deafness-associated m.7445T>C mutation in the precursor of $tRNA^{Ser(UCN)}$ and cardiomyopathy-associated $tRNA^{Ile}$ 4269A>G and 4295A>G mutations, and $tRNA^{His}$ 12192G>A mutation perturbed the 3′ end processing of corresponding tRNA precursors (19–21). The $tRNA^{Ile}$ 4263A>G and $tRNA^{Ala}$ 5655A>G mutations at the 5′ end (conventional position 1) of corresponding tRNAs altered the 5′ end processing of $tRNA^{Ile}$ and $tRNA^{Ala}$ precursors, respectively (24,25). Strikingly, the m.4401A>G mutation at the junction of $tRNA^{Met}$ and $tRNA^{Gln}$ genes caused the 5′ end aberrant processing of $tRNA^{Met}$ in the H-strand transcripts and $tRNA^{Gln}$ as well as other seven tRNAs and ND6 mRNA in the L-strand transcripts (26). These suggested the asymmetrical processing mechanisms of H-strand and L-strand polycistronic transcripts (26). However, the pathogenic mechanisms underlying these tRNA processing defects remain elusive.

Most recently, we identified the m.7516delA mutation in one Han Chinese family with maternal inheritance of deafness in a large cohort of Chinese hearing-impaired probands (27). As shown in Figure 1, the nucleotide at position 7516 resided at 3 bp (AAA/TTT) spacers to 5′ ends

of $tRNA^{Asp}$ and $tRNA^{Ser(UCN)}$, respectively (4,12,27,28). It was likely that the (AAA/TTT) spacers were the 5′ end processing sites of $tRNA^{Asp}$ and $tRNA^{Ser(UCN)}$, recognized by RNase P, for both H-strand transcript and L-strand transcript precursors, respectively. Therefore, we hypothesized that the m.7516delA mutation perturbed the 5′ end processing of $tRNA^{Asp}$ at the H-strand transcript and the $tRNA^{Ser(UCN)}$ at the L-strand transcript, thereby causing the decrease of tRNAs and mRNAs. It was also anticipated that the failures in tRNA metabolism resulted in the impairment of mitochondrial translation, defects in oxidative phosphorylation, oxidative stress and subsequent failure of cellular energetic processes. To elucidate pathogenic mechanism of m.7516delA mutation, we generated the cytoplasmic hybrids (cybrids) by transferring mitochondria from lymphoblastoid cell lines derived from a hearing-impaired proband carrying the m.7516delA mutation and from a control subject lacking the mutation but belonging to same mtDNA haplotype into mtDNA-less ρ°206 cells (29–31). The resultant cybrids under these constant nuclear and mitochondrial genetic backgrounds allowed us to evaluate the specific effects of mtDNA mutation(s) on functional consequences for the pathological process (30–32). These cybrid lines were analyzed for the effects of the m.7516delA mutation on the processing and stability of mitochondrial tRNA and mRNA, mitochondrial translation, respiration, mitochondrial membrane potential, production of reactive oxidative species (ROS) and apoptosis.

MATERIALS AND METHODS

Subjects and audiological examinations

A hearing-impaired Han Chinese family was recruited from the Shandong Provincial ENT Hospital, Shangdong University, as described previously (Supplementary Figure S1) (27). Comprehensive history-taking, physical examination and audiological examination were performed to identify any syndromic findings, history of exposure to aminoglycosides and genetic factors related to hearing impairment in all available members of this Chinese pedigree, as detailed previously (33,34). Informed consent, blood samples and clinical evaluations were obtained from all participating family members under protocols approved by the Ethics Committees of Zhejiang University and Shandong University.

Analysis of mitochondrial DNAs

Genomic DNA was isolated from whole blood of participants using QIAamp DNA Blood Mini Kit (Qiagen, No. 51104). The subjects' DNA fragments spanning the mitochondrial $tRNA^{Asp}$ and $tRNA^{Ser(UCN)}$ genes were PCR amplified by use of oligodeoxynucleotides corresponding to mtDNA at 7129–7148 and 8095–8114 (4). Fragment was purified and then analyzed by direct sequencing. These sequence results were compared with the updated consensus Cambridge sequence (GenBank accession number: NC_012920) (35). The entire mtDNAs of the proband III-3 and one Chinese control subject (C17) belonging to the same mtDNA haplotype were PCR amplified in 24 overlapping fragments using sets of the L- and H-strand oligonucleotide primers, as described previously (36). These sequence results were compared with the updated consensus Cambridge sequence, as described earlier.

Cell lines and culture conditions

Lymphoblastoid cell lines were immortalized by transformation with the Epstein–Barr virus, as described elsewhere (37). Cell lines derived from one affected matrilineal relative (III-3) of the Chinese family carrying the m.7516delA mutation and one genetically unrelated control individual (C17) lacking the mutation (Supplementary Table S1) were grown in the RPMI 1640 medium (Invitrogen) supplemented with 10% fetal bovine serum (FBS). The bromodeoxyuridine (BrdU)-resistant 143B.TK$^-$ cell line was grown in Dulbecco's modified Eagle medium (Life Technologies) (containing 4.5 mg of glucose and 0.11 mg of pyruvate/ml), supplemented with 100 μg of BrdU/ml and 5% FBS. The mtDNA-less ρ°206 cell line, derived from 143B.TK$^-$ cells, was grown under the same conditions as the parental line, except for the addition of 50 μg of uridine/ml. All cybrid cell lines constructed with enucleated lymphoblastoid cell lines were maintained in the same medium as the 143B.TK$^-$ cell line. The generation of cybrid cell lines from III-3 and C17 by cytoplasts of mtDNA-less ρ°206 cells was performed as detailed elsewhere (29–31). The presence and level of m.7516delA mutation and mtDNA copy numbers in cybrid cell lines were analyzed as detailed elsewhere (38). Three mutant cybrids (III-3.1, III-3.2 and III-3.3) carrying the homoplasmic m.7516delA mutation and three control cybrids (C17.1, C17.2 and C17.3) lacking the mutation with similar mtDNA copy numbers were used for the biochemical characterization.

Mitochondrial RNase P cleavage assay

The wild-type and mutant precursors of $tRNA^{Asp}$ corresponding to mtDNA at positions 7478 (5′) to 7613 (3′), and $tRNA^{Ser(UCN)}$ at mtDNA positions 7550 (5′) to 7419 (3′) were cloned into the pCRII-TOPO vector carrying SP6 and T7 promoters (Clontech). After HindIII digestion, the labeled RNA substrates (136 nt for $tRNA^{Asp}$ and 132 nt for $tRNA^{Ser(UCN)}$) were transcribed with T7 RNA polymerase, in the presence of 10 μM ATP, CTP, GTP and UTP, pH 7.5, and 10 units of RNase inhibitor at 37°C. Transcripts were purified by denaturing polyacrylamide gel electrophoresis (PAGE) [8 M urea, 8% polyacrylamide/bisacrylamide (19:1)] and were dissolved in 1 mM EDTA. Mitochondrial RNase P was reconstituted from purified recombinant proteins MRPP1, MRPP2 and MRPP3 as described previously (15,26). The reaction mixture was incubated in 40 μl assay buffer containing 20 mM HEPES (pH 7.6), 20 mM KCl, 2 mM $MgCl_2$, 2 mM DTT, 0.1 mg/ml bovine serum albumin, 80 μM *S*-adenosyl methionine, 1 U RiboLock RNase Inhibitor (Thermo Fisher Scientific), 300 ng pre-tRNAs, 800 nM MRPP1/2 and 100 nM MRPP3. The reaction mixes were pre-incubated at 30°C for 15 min, and the reaction was initiated by addition of MRPP3 and pre-tRNA substrates with subsequent incubation at 30°C. After 5, 10, 15, 20, 25 and 40 min, 5 μl of aliquots were withdrawn and stopped by addition of 5 μl loading buffer (85% formamide, 10 mM

EDTA). The reaction products were separated by denaturing 10% PAGE in 1× Tris–borate–EDTA (TBE) buffer. After electrophoresis, the reaction products were visualized by staining with NA-Red (Beyotime).

Mitochondrial RNA analysis

Total RNAs were obtained by using TOTALLY RNA™ kit (Ambion) from intact cells or mitochondria isolated from mutant and control cell lines (~2 × 10^8 cells), as detailed elsewhere (39). For tRNA Northern blot analysis, 6 μg of total cellular RNA was electrophoresed through a 10% polyacrylamide/8 M urea gel in 1× TBE buffer after heating the samples at 65°C for 10 min, and then electroblotted onto a positively charged Nylon membrane (Roche) for the hybridization analysis with digoxigenin (DIG)-labeled oligodeoxynucleotide probes, respectively. A set of DIG-labeled probes of 22 mitochondrial tRNAs and 5S rRNA was described elsewhere (26,40,41). The hybridization and quantification of density in each band were performed as detailed previously (40–43).

For mRNA Northern blot analysis, 6 μg of total cellular RNA was fractionated by electrophoresis through a 2% agarose–formaldehyde gel, transferred onto a positively charged membrane (Roche) and hybridized with a set of DIG-labeled RNA probes: COX2, CYTB, ND1, ND3, ND6, COX1, 12S rRNA, 16S rRNA and β-actin as a control, respectively. Probes were synthesized as described previously (13,26,44). The hybridization and quantification of density in each band were performed as detailed previously (26,44).

Western blot analysis

Western blot analysis was performed as detailed previously (40,45,46). Twenty micrograms of total cell proteins obtained from various cell lines were denatured and loaded on sodium dodecyl sulfate polyacrylamide gels. The gels were electroblotted onto a polyvinylidene difluoride membrane for hybridization. The antibodies obtained from different companies were as follows: Abcam [TOM20 (ab56783), ND1 (ab74257), ND5 (ab92624), CO1 (ab695), CO2 (ab110258), ND6 (ab81212), Total OXPHOS Human WB Antibody Cocktail (ab110411) and CYTC (ab13575)], Cell Signaling Technology [Cleaved Caspase 3 (#9664), Cleaved Caspase 9 (#7237), Cleaved PARP (#5625), SOD1 (4266T), SOD2 (13141T) and Catalase (12980T)], Novus [ND4 (NBP2-47365)] and Proteintech [CYTB (55090-1-AP), ATP8 (26723-1-AP), CO3 (55082-1-AP), Afg3l2 (14631-1-AP), Clpp (15698-1-AP), Lonp1 (66043-1-AP) and GAPDH (10494-1-AP)]. Peroxidase AffiniPure goat anti-mouse IgG and goat anti-rabbit IgG (Jackson) were used as a secondary antibody and protein signals were detected using the ECL system (CWBIO). Quantification of density in each band was performed as detailed previously (40,45,46).

Measurements of oxygen consumption

The oxygen consumption rates (OCRs) in cybrid cell lines were measured with a Seahorse Bioscience XF-96 Extracellular Flux Analyzer (Seahorse Bioscience), as detailed elsewhere (46,47).

Enzymatic assays

The enzymatic activities of complex I (NADH ubiquinone oxidoreductase), complex II (cytochrome *c*), complex III (ubiquinone cytochrome *c* oxidoreductase) and complex IV (cytochrome *c* oxidase) were assayed as detailed previously (46,48,49).

Assessment of mitochondrial membrane potential

Mitochondrial membrane potential from various cybrid cell lines was examined with JC-10 Assay Kit-Flow Cytometry (Abcam) following general manufacturer's recommendations with some modifications, as detailed elsewhere (40,50).

Measurement of ROS production

The levels of ROS generation by mitochondria in various cell lines were analyzed using the mitochondrial superoxide indicator MitoSOX-Red following the procedures as detailed previously (25,51–53).

Apoptosis assay

Apoptosis in the cybrids treated with or without gentamycin was determined using the Annexin V-FITC Apoptosis Kit (Bio Legend, 640914) according to manufacturer's protocol (53). A total of 1 × 10^6 cells/ml were seeded in six-well culture plates and treated with or without gentamycin for 24 h. Then, all of the harvested cells were stained with Annexin V and propidium iodide (PI) for 15 min at room temperature and subsequently analyzed via flow cytometry (FACS Calibur, BD Biosciences). The data were analyzed using FlowJo software, as detailed elsewhere (52).

Statistics analysis

Statistical analysis was performed using GraphPad Prism (version 8.0.2) to compare outcomes using a two-tailed paired and unpaired Student's *t*-test. For multiple comparisons, two-way ANOVA analysis was performed. *P*-values <0.05 were considered to be statistically significant.

RESULTS

Clinical presentation of one Chinese family

One Han Chinese hearing-impaired proband carrying the m.7516delA mutation was identified among 887 Chinese hearing-impaired probands and 773 Chinese hearing normal controls (27). As shown in Supplementary Figure S1 and Supplementary Table S2, the Chinese family exhibited the maternal inheritance of hearing loss. As shown in Supplementary Figure S2, all matrilineal relatives exhibited variable degree of hearing impairment (three individuals with severe hearing loss and two subjects with moderate hearing loss). The age at onset of hearing loss ranged from 17 to 20 years, with an average age of 18 years. These

matrilineal relatives exhibited no other clinical abnormalities, including cardiac failure, muscular diseases, visual loss and neurological disorders. There was no evidence that any member of this family had any other known causes to account for hearing impairment. Further analysis showed that the m.7516delA mutation was present in homoplasmy in the all matrilineal relatives but not in other members of this family (Supplementary Table S2).

The aberrant 5′ end processing of tRNA^{Asp} and tRNA$^{Ser(UCN)}$ precursors

To examine whether the m.7516delA mutation altered the 5′ end processing efficiencies of tRNA^{Asp} from the H-strand transcripts and tRNA$^{Ser(UCN)}$ from the L-strand transcripts, we performed an *in vitro* processing experiment using RNase P that was reconstituted from purified recombinant proteins MRPP1, MRPP2 and MRPP3 as described previously (15,25,26). As illustrated in Figure 2A and B, the wild-type and mutant tRNA^{Asp} and tRNA$^{Ser(UCN)}$ precursors corresponding to mtDNA at positions 7478–7613 and 7550–7419 were prepared by *in vitro* transcription, respectively. To analyze the *in vitro* processing kinetics, the wild-type and mutant tRNA^{Asp} and tRNA$^{Ser(UCN)}$ precursors were incubated with RNase P at various time courses. The relative processing efficiencies were calculated by the ratios of cleaved pre-tRNAs at the plateau phase according to the fitted curve under exponential equation (one-phase association). As shown in Figure 2C–F, the processing efficiencies of the mutant tRNA^{Asp} and tRNA$^{Ser(UCN)}$ transcripts were significantly reduced, as compared with those of wild-type counterparts. In particular, the processing efficiencies of mutant tRNA^{Asp} and tRNA$^{Ser(UCN)}$ transcripts catalyzed by RNase P were ∼67% and ∼53% of those in their wild-type counterparts (Figure 2E and F), respectively. These results demonstrated that the m.7516delA mutation perturbed the 5′ end processing of tRNA^{Asp} and tRNA$^{Ser(UCN)}$ precursors.

Reduced levels of tRNA^{Asp} from H-strand transcripts and six tRNAs from L-strand transcripts

To test the hypothesis that the aberrant 5′ end processing of tRNA^{Asp} and tRNA$^{Ser(UCN)}$ by the m.7516delA mutation affected other tRNA processing and subsequently reduced the levels of tRNAs, we subjected total cellular RNAs from mutant and control cell lines to Northern blots and hybridized them with DIG-labeled oligodeoxynucleotide probes for 14 tRNAs including tRNA^{Asp}, tRNA^{Lys}, tRNA$^{Leu(UUR)}$ and tRNA$^{Ser(AGY)}$ derived from the H-strand transcripts and 8 tRNAs including tRNA$^{Ser(UCN)}$ derived from the L-strand transcripts (7,13,26). As shown in Figure 3, the average levels of tRNA^{Asp} and tRNA$^{Ser(UCN)}$ in three mutant cybrids were 53% and 44% ($P < 0.01$) of the mean values of three control cybrids, respectively. Strikingly, the average steady-state levels of five tRNAs, downstream of tRNA$^{Ser(UCN)}$ from the L-strand transcripts, were significantly decreased. Especially, the average levels of tRNA^{Tyr}, tRNA^{Cys}, tRNA^{Asn}, tRNA^{Ala} and tRNA^{Gln} in three mutant cybrids were 48%, 51%, 47%, 51% and 46% of those in three control cybrids, respectively. However, the levels of tRNA^{Pro} and tRNA^{Glu} from upstream of tRNA$^{Ser(UCN)}$ in the L-strand transcripts and other 13 tRNAs including tRNA^{Lys}, tRNA$^{Leu(CUN)}$ and tRNA$^{Ser(AGY)}$ from the H-strand transcripts in the mutant cybrids were comparable with those in three control cybrids. These data indicated that the m.7516delA mutation led to the asymmetrical defects of tRNAs from H-strand and L-strand transcripts, respectively.

Aberrant processing of COX2 mRNA precursor

We then examined whether the m.7516delA mutation perturbed the processing of mRNA, 12S rRNA and 16S rRNA, and caused the accumulation of longer and uncleaved precursors. RNA transfer hybridization experiments were performed with total cellular RNAs from various mutant and control cybrids, using a set of DIG-labeled RNA probes: ND6 from L-strand transcript, ND1, ND3, COX1, COX2, CYTB, 12S rRNA and 16S rRNA from H-strand transcript (13,26) and β-actin as a control. As shown in Figure 4A and B, two RNA species with ∼0.83 and ∼0.7 kb long were detected using COX2 probe in both mutant and control cell lines. As shown in Figure 4B, the analyses using both tRNA^{Asp} and anti-tRNA$^{Ser(UCN)}$ probes only detected one RNA with ∼0.83 kb long. The ∼0.7 kb RNA was equal in size to 684-nt coding sequence of COX2 mRNA. Thus, the 0.83 kb RNA could conceivably be a precursor of COX2 mRNA, consisting of 72-nt noncoding sequence (7446–7517), 68-nt coding sequence of tRNA^{Asp} (7518–7585) and 684-nt coding sequence of COX2. To verify the putative COX2 mRNA, three cDNA fragments [684 bp (COX2 coding sequence at positions 7586–8269), 755 bp (at positions 7515–8269) and 824 bp (at positions 7446–8269)] from the control cell line C17.1 and mutant cell line III-3.1 were analyzed by Sanger sequencing after cDNA synthesis and PCR amplification (Supplementary Figure S3). Indeed, all three fragments contained the identical 684 bp COX2 coding sequence, while 755 bp harboring 68-nt coding sequence of tRNA^{Asp} and 3 bp noncoding sequence and 824 bp fragments encompassed the 68-nt coding sequence of tRNA^{Asp} and coding sequence and 5′ untranslated sequences. This result confirmed that ∼0.7 kb RNA was indeed COX2 mRNA. As shown in Figure 4A and D, the mutant cell lines displayed decreased levels of COX2 mRNA but accumulated precursors of COX2, as compared with those in the control cell lines. The average levels of COX2 mRNA and its precursors in three mutant cybrids, normalized with respect to those of β-actin mRNA, were 68.5% and 130.1% of those in the control cell lines, respectively ($P < 0.01$). However, the levels of ND1, ND3, COX1, CYTB, 12S rRNA and 16S rRNA from H-strand transcripts and ND6 from L-strand transcripts in mutant cybrids, normalized with respect to those of β-actin mRNA, were comparable with those in the control cell lines (Figure 4C and Supplementary Figure S4). These results demonstrated that the m.7516delA mutation perturbed the processing of COX2 mRNA precursors but did not affect the processing of other mRNAs and rRNAs from the H-strand and L-strand transcripts.

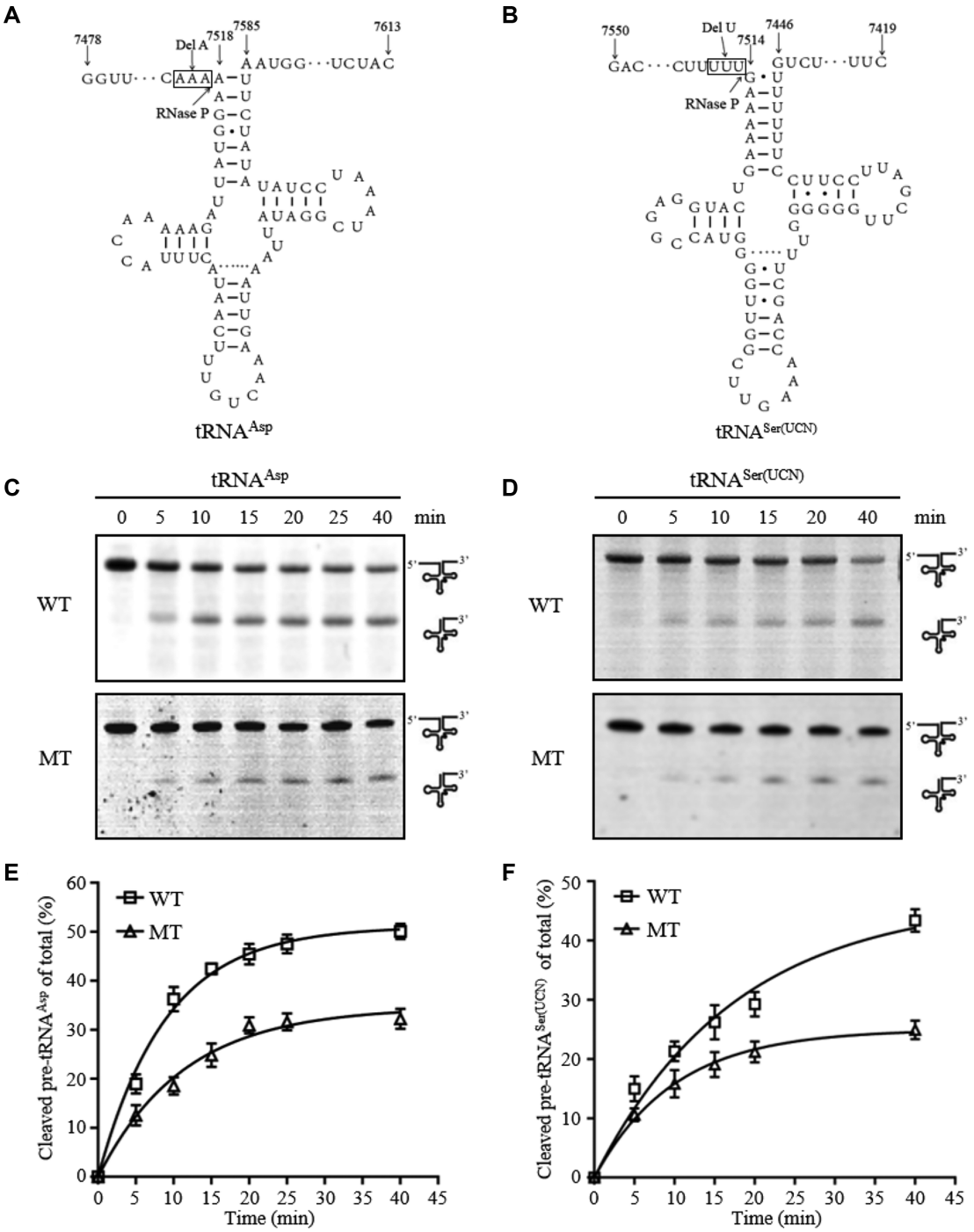

Figure 2. *In vitro* assay for the processing of $tRNA^{Ser(UCN)}$ and $tRNA^{Asp}$ precursors. (**A, B**) Mitochondrial $tRNA^{Ser(UCN)}$ and $tRNA^{Asp}$ precursors. Forty and 36 nucleotides (nt) of 5′ end leaders, and 28 and 27 nt of the 3′ end trailer of $tRNA^{Ser(UCN)}$ and $tRNA^{Asp}$ were shown, respectively. (**C, D**) *In vitro* processing assays. Processing assays with RNase P were carried out in parallel for wild-type and mutant substrates. Samples were withdrawn and stopped after 5, 10, 15, 20 or 40 min, respectively. Reaction products were resolved by denaturing PAGE and were visualized by staining with NA-Red (Beyotime). (**E, F**) Quantification of the efficiencies of $tRNA^{Ser(UCN)}$ and $tRNA^{Asp}$ precursors catalyzed by RNase P. The relative processing efficiencies were calculated by the ratios of cleaved pre-tRNAs at the plateau phase according to the fitted curve under exponential equation (one-phase association). The calculations were based on four independent determinations. The error bars indicate two standard errors of the mean.

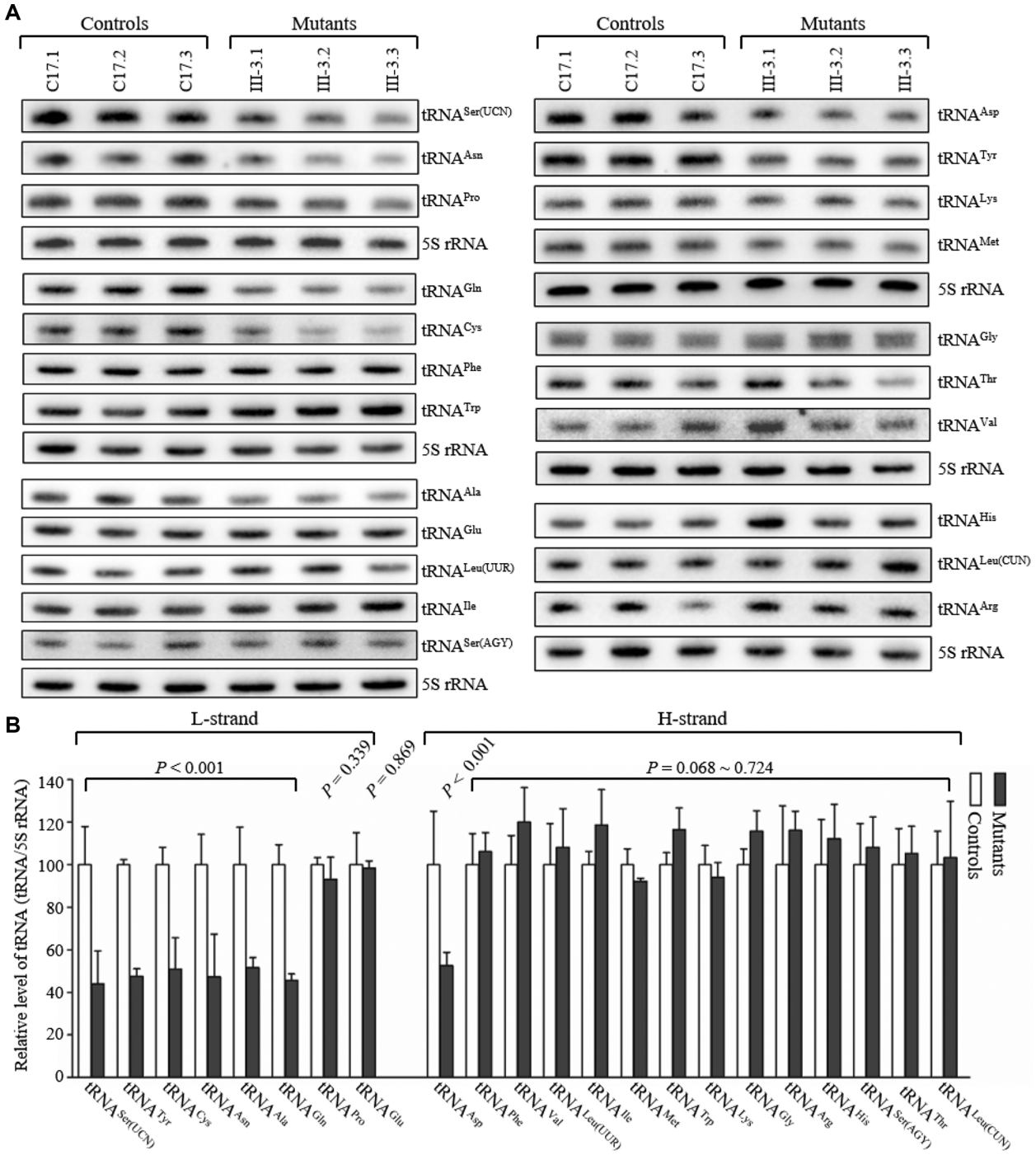

Figure 3. Northern blot analysis of mitochondrial tRNAs. (**A**) Six micrograms of total cellular RNAs from the various cell lines were electrophoresed through a 10% denaturing polyacrylamide gel, electroblotted and hybridized with DIG-labeled oligonucleotide probes specific for $tRNA^{Ser(UCN)}$, $tRNA^{Asn}$, $tRNA^{Pro}$, $tRNA^{Gln}$, $tRNA^{Cys}$, $tRNA^{Tyr}$, $tRNA^{Ala}$ and $tRNA^{Glu}$ from the L-strand transcripts, $tRNA^{Asp}$, $tRNA^{Phe}$, $tRNA^{Val}$, $tRNA^{Leu(UUR)}$, $tRNA^{Ile}$, $tRNA^{Met}$, $tRNA^{Trp}$, $tRNA^{Lys}$, $tRNA^{Gly}$, $tRNA^{Arg}$, $tRNA^{His}$, $tRNA^{Ser(AGY)}$, $tRNA^{Leu(CUN)}$ and $tRNA^{Thr}$ from the H-strand transcripts, and 5S rRNA, respectively. (**B**) Quantification of the tRNA levels. Average relative each tRNA content per cell was normalized to the average content per cell of 5S rRNA in the control and mutant cybrids, respectively. The values for the latter were expressed as percentages of the average values for the control cybrids. The calculations were based on three independent determinations in each cybrids. The error bars indicate two standard errors of the mean. *P* indicates the significance, according to the *t*-test, of the difference between mutant and control cybrids.

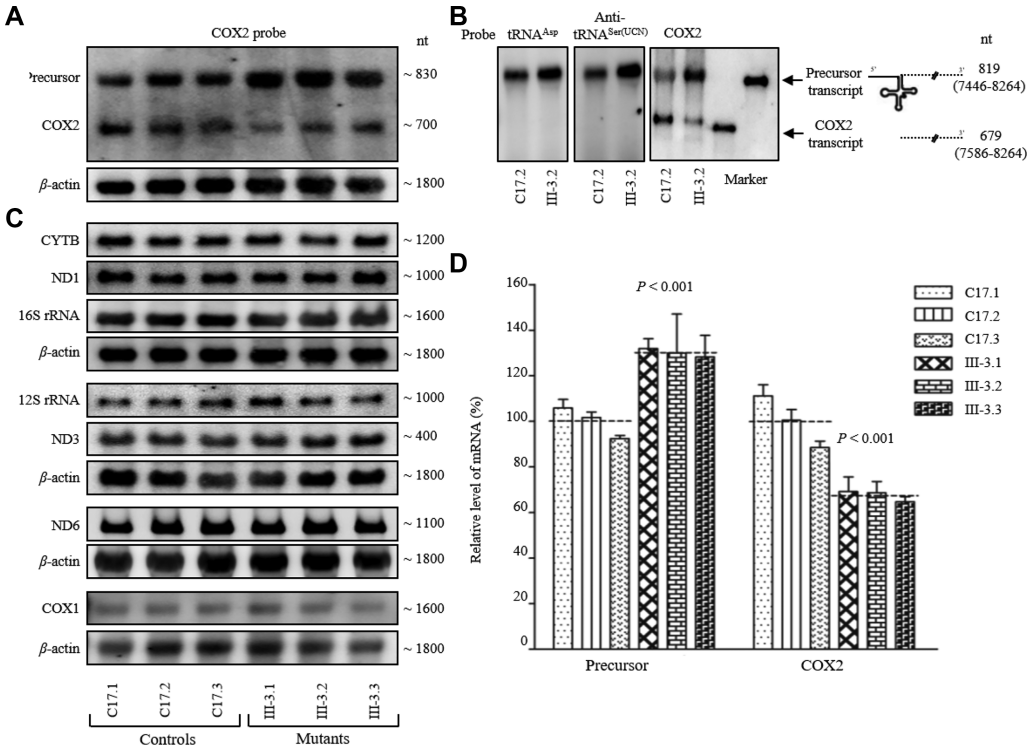

Figure 4. Northern blot analysis of mitochondrial RNAs. (**A–C**) Six micrograms of total cellular RNAs from various cybrids were electrophoresed through a 2% agarose–formaldehyde gel, transferred onto a positively charged membrane and hybridized with DIG-labeled RNA probes for COX2 (**A**); COX2, $tRNA^{Asp}$ and anti-$tRNA^{Ser(UCN)}$ (**B**); ND1, ND3, ND6, COX1, CYTB, 12S rRNA and 16S rRNA (**C**); and β-actin as a loading control. (**D**) Average relative levels of COX2 mRNA and precursors per cell were normalized to the average level per cell of β-actin in three control cybrids and three mutant cybrids. The values for the latter were expressed as percentages of the average values for the control cell lines. Three independent determinations were used in the calculations. Graph details and symbols are explained in the legend to Figure 3.

The impairment of mitochondrial translation

To examine whether the m.7516delA mutation impaired mitochondrial translation, a Western blot analysis was carried out to examine the levels of nine mtDNA-encoded polypeptides [ND1, ND4, ND5 and ND6 (subunits 1, 4, 5 and 6 of NADH dehydrogenase), CO1, CO2, CO3 (subunit I, II and III of cytochrome *c* oxidase), CYTB (apocytochrome b) and ATP8 (subunit 8 of H^+-ATPase)] in mutant and control cybrids with a nucleus-encoded mitochondrial protein TOM20 as a loading control. As shown in Figure 5A and B, the overall levels of nine mitochondrial translation products in the mutant cell lines were 71.6% ($P < 0.001$), relative to the mean value measured in the control cell lines. The average levels of ND1, ND4, ND5, ND6, CO1, CO2, CO3, ATP8 and CYTB in the mutant cells were 116.5%, 43.1%, 39.6%, 114.9%, 50.9%, 60.6%, 49.3%, 92.6% and 92.3% of those in the control cell lines after normalization to TOM20, respectively.

We then examined the levels of five subunits (CO2, NDUFB8 of NADH:ubiquinone oxidoreductase, SDHB of succinate ubiquinone oxidoreductase, UQCRC2 of ubiquinol cytochrome *c* reductase and ATP5A of H^+-ATPase, encoded by nuclear genes) of the phosphorylation system (OXPHOS) in the control and mutant cybrids. As shown in Supplementary Figure S5, the average levels of CO2 in the mutant cells were 65.6% ($P = 0.018$) of control cell lines, while the levels of NDUFB8, SDHB, UQCRC2 and ATP5A in the mutant cell lines were comparable with those in control cell lines.

The m.7516delA mutation induced proteostasis stress

To test whether the m.7516delA mutation-induced deficiency affected the mitochondrial proteostasis, we measured the levels of Lonp1 involved in the maintenance of mitochondrial proteostasis and gene expression (54), Clpp involved in mitochondrial ribosome assembly (55) and ATP family gene 3-like2 (Afg3l2) proteases involved in the turnover of misfolded protein markers for proteostasis stress (56), in the mutant and control cybrids. As shown in Figure 5C and D, the levels of Lonp1, Afg3l2 and Clpp in the mutant cells were 136.2% ($P < 0.01$), 160.8% ($P < 0.01$) and 153.6% ($P < 0.01$) of those in the control cell lines after normalization to GAPDH, respectively. These data indicated that m.7516delA mutation induced the proteostasis stress.

Deficient activities of respiratory chain complexes

To evaluate whether the impairment of mitochondrial translation caused the deficient oxidative phosphorylation, we measured the activities of respiratory complexes by the use of isolated mitochondria from mutant and control cell lines. The activity of complex I (NADH ubiquinone oxidoreductase) was determined through the oxidation of

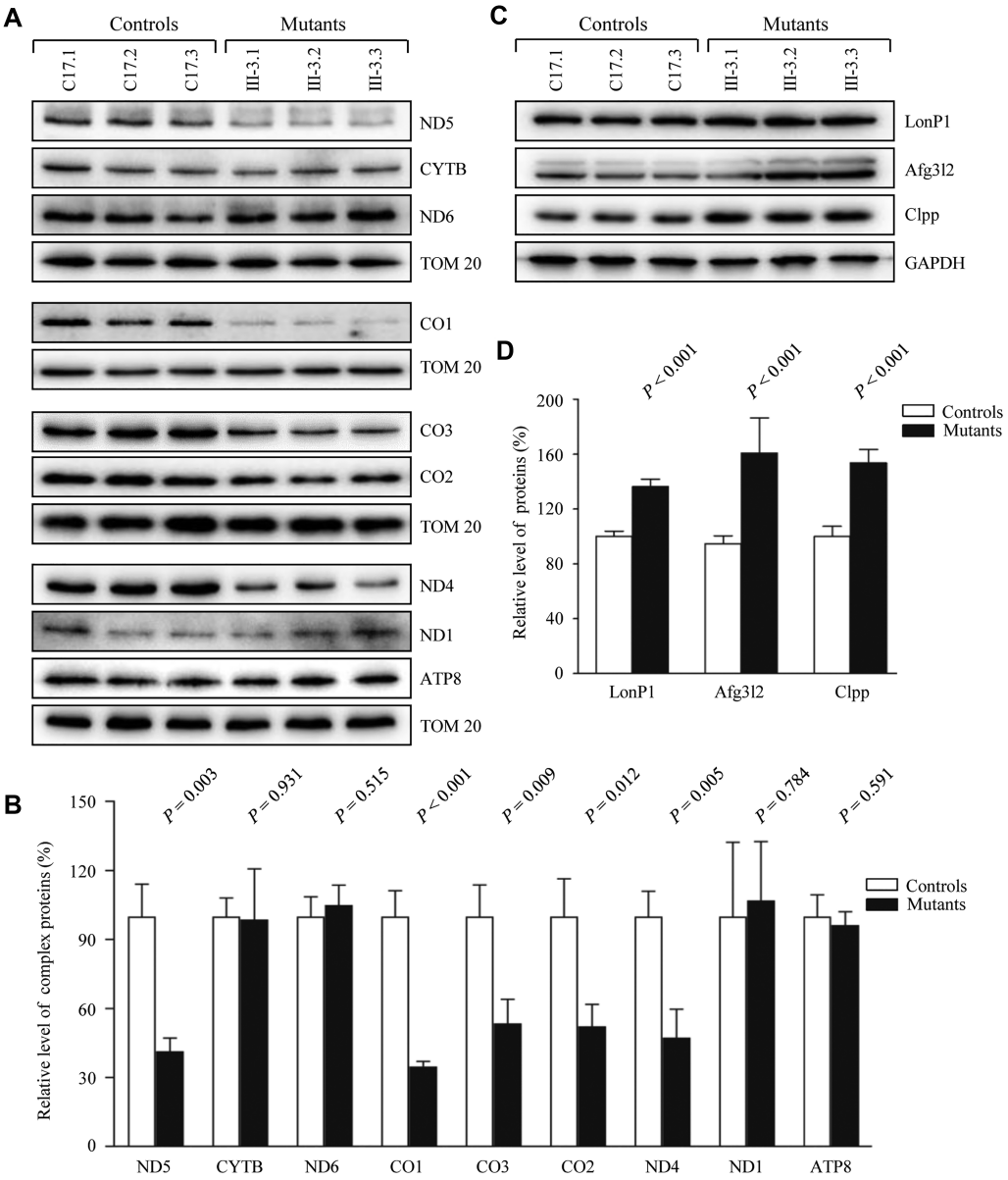

Figure 5. Analysis of mitochondrial translation and proteostasis stress. (**A**) Analysis of mtDNA-encoded proteins. Five micrograms of total mitochondrial proteins from various cybrids were electrophoresed through a denaturing polyacrylamide gel, electroblotted and hybridized with antibodies specific for ND1, ND4, ND5, ND6, CO1, CO2, CO3, CYTB and ATP8, with TOM20 as a loading control. (**B**) Quantification of nine polypeptides. The average relative values of ND1, ND4, ND5, ND6, CO1, CO2, CO3, CYTB and ATP8 in mutant and control cell lines were normalized to the average values of TOM20 in various cell lines. The values for the latter are expressed as percentages of the average values for the control cell lines. The calculations were based on three independent determinations. For multiple comparisons, two-way ANOVA was performed. (**C**) Western blotting analysis of LonP1, Afg3l2 and Clpp proteins. Twenty micrograms of total cellular proteins from various cybrids were electrophoresed through a denaturing polyacrylamide gel, electroblotted and hybridized with antibodies for LonP1, Afg3l2 and Clpp as well as GAPDH as a loading control. (**D**) Quantification of levels of LonP1, Afg3l2 and Clpp. The calculations were based on three independent experiments. Graph details and symbols are explained in the legend to Figure 3.

NADH with ubiquinone as the electron acceptor (57,58). The activity of complex II (succinate ubiquinone oxidoreductase) was examined through the artificial electron acceptor DCPIP. The activity of complex III (ubiquinone cytochrome *c* oxidoreductase) was measured through the reduction of cytochrome *c* by using D-ubiquinol-2 as the electron donor. The activity of complex IV (cytochrome *c* oxidase) was monitored through the oxidation of cytochrome *c*. Complex I–IV activities were normalized by citrate synthase activity. As shown in Figure 6A, the average activities of complexes I and IV in three mutant cybrids were 69.7% ($P < 0.001$) and 66.3% ($P < 0.001$) of the mean values measured in three control cybrids, respectively. However, the average activities of complexes II and III in three mutant cybrids were 99.1% ($P = 0.801$) and 95.7% ($P = 0.263$) of the mean values measured in three control cybrids, respectively.

Furthermore, we measured the OCRs of various mutant and control cybrid cell lines using a Seahorse Bioscience XF-96 Extracellular Flux Analyzer (47). As shown in Figure 6B and C, the average basal OCRs in three mutant cy-

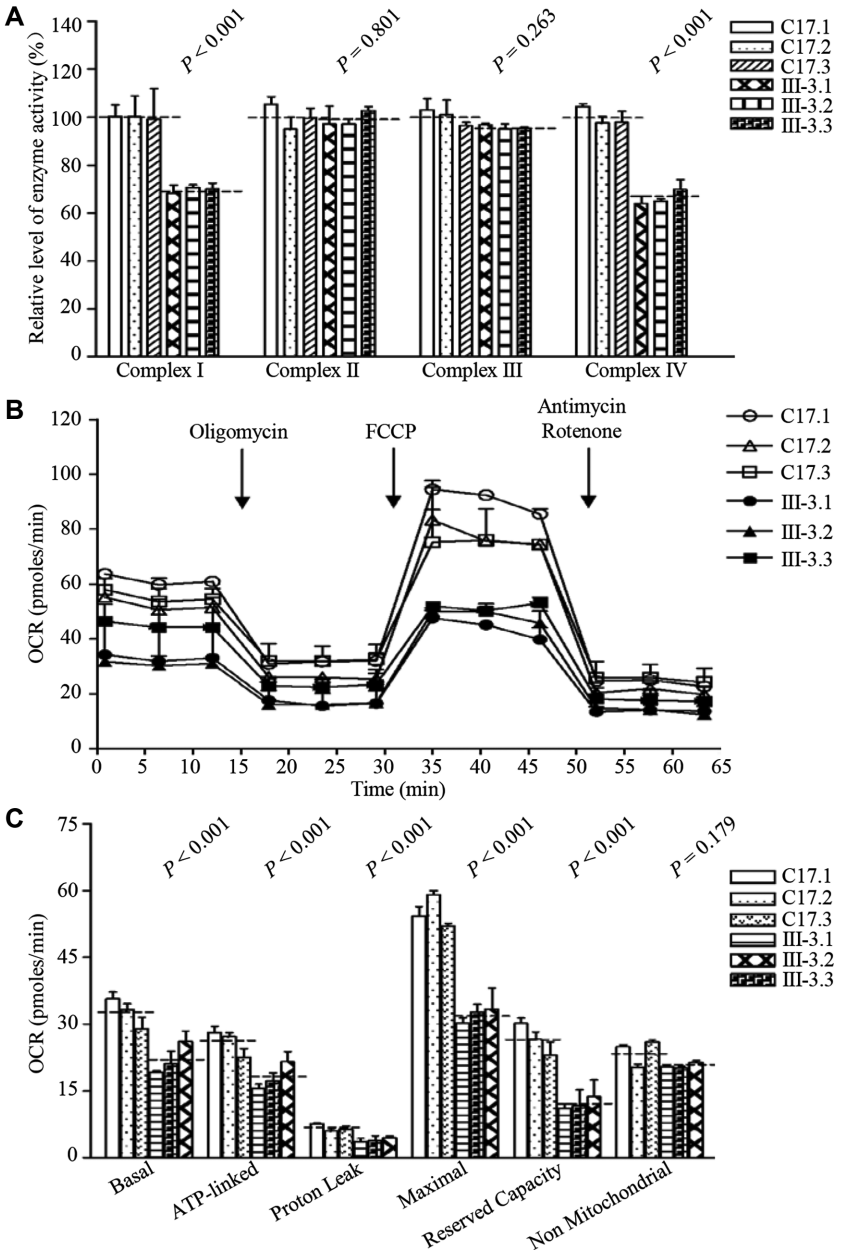

Figure 6. Respiration and enzymatic activities assays. (**A**) Enzymatic activities of respiratory chain complexes. The activities of respiratory complexes were investigated by an enzymatic assay on complexes I, II, III and IV in mitochondria isolated from various cell lines. The calculations were based on three independent determinations. (**B**) An analysis of O_2 consumption rate (OCR) in the various cell lines using different inhibitors. The OCRs were first measured on 1×10^4 cells of each cell line under basal condition and then sequentially added oligomycin (1.5 μM), carbonyl cyanide *p*-(trifluoromethoxy)phenylhydrazone (FCCP) (0.5 μM), rotenone (1 μM) and antimycin A (1 μM) at indicated times to determine different parameters of mitochondrial functions. (**C**) Graphs presented the ATP-linked OCR, proton leak OCR, maximal OCR, reserve capacity OCR and non-mitochondrial OCR in mutant and control cell lines. Non-mitochondrial OCR was determined as the OCR after rotenone/antimycin A treatment. Basal OCR was determined as OCR before oligomycin minus OCR after rotenone/antimycin A. ATP-linked OCR was determined as OCR before oligomycin minus OCR after oligomycin. Proton leak OCR was determined as basal OCR minus ATP-linked OCR. Maximal OCR was determined as the OCR after FCCP minus non-mitochondrial OCR. Reserve capacity OCR was defined as the difference between maximal OCR after FCCP minus basal OCR. The average values of three determinations for each cell line are shown. Graph details and symbols are explained in the legend to Figure 3.

brids were 67.7% ($P < 0.01$) of the mean values measured in three control cybrids. To further investigate which of the enzyme complexes of the respiratory chain was affected in the mutant cybrids, OCR was measured after the sequential addition of oligomycin (to inhibit the ATP synthase), FCCP (to uncouple the mitochondrial inner membrane and allow for maximum electron flux through the ETC), antimycin A (to inhibit complex III) and rotenone (to inhibit complex I). As shown in Figure 6C, the ATP-linked OCR, proton leak OCR, maximal OCR, reserve capacity OCR and non-mitochondrial OCR in mutant cybrids were 69.9% ($P < 0.001$), 59.2% ($P < 0.0.001$), 58.3% ($P < 0.001$), 45.7% ($P < 0.001$) and 86.9% ($P = 0.179$), relative to the mean values measured in the control cybrids, respectively.

Decreases in mitochondrial membrane potential

The mitochondrial membrane potential ($\Delta\Psi_m$) generated by proton pumps (complexes I, III and IV) is an essential component in the process of energy storage during oxidative phosphorylation (40,50). The mitochondrial membrane potentials ($\Delta\Psi_m$) of mutant and control cybrids were examined through the fluorescence probe JC-10 assay system. The ratios of fluorescence intensities Ex/Em = 490/590 and 490/530 nm (FL590/FL530) were recorded to delineate the $\Delta\Psi_m$ of each sample. The relative ratios of FL590/FL530 geometric mean between mutant and control cybrids were calculated to represent the level of $\Delta\Psi_m$, as described elsewhere (46,50). As illustrated in Figure 7, $\Delta\Psi_m$ of three mutant cybrids ranged from 53.2% to 59.8%, with an average 57.1% ($P < 0.001$) of the mean value measured in three control cybrids. In contrast, the levels of $\Delta\Psi_m$ in three mutant cell lines in the presence of FCCP were comparable to those of three control cell lines.

The increase of mitochondrial ROS production

Mitochondrial ROS are gradually recognized as important signaling mediators in a wide range of cellular processes (59). To test whether the m.7516delA mutation elevated the production of mitochondrial ROS, the levels of mitochondrial ROS generation in the mutant and control cybrids were determined using the MitoSOX assay via flow cytometry (25,51,52). Geometric mean intensity was recorded to measure the production rate of ROS of each sample. As shown in Figure 8A and B, the levels of ROS generation in the mutant cybrids ranged from 132.6% to 136.3%, with an average of 134.1% ($P < 0.01$) of the mean values measured in the control cybrids under unstimulated conditions.

To access whether the m.7516delA mutation-induced mitochondrial ROS production affected the antioxidant systems, we examined the levels of three antioxidant enzymes: SOD2 in mitochondria, and SOD1 and catalase in cytosol in the various cell lines (45,59,60). As shown in Figure 8C and D, the mutant cell lines revealed marked increases in the levels of SOD2 (152.1%), SOD1 (182.7%) and catalase (164.3%), as compared with those in the control cybrids.

Promoting apoptosis

Deficient activities of oxidative phosphorylation have been linked to protect against certain apoptotic stimuli (31,61). To assess whether the m.7516delA mutation affects the apoptotic processes, we examined the apoptotic state of mutant and control cybrids by Annexin V-FITC/PI assay using the flow cytometry (53) and Western blot analyses. As shown in Figure 9A and B, the levels of early and late apoptosis in the mutant cybrids carrying the m.7516delA mutation ranged from 204.8% to 226.7%, with an average of 214.9% ($P < 0.001$) of the mean values measured in the control cybrids.

Cytochrome *c* released from mitochondria recruits and activates apoptosis-activated proteins such as procaspase 9 and then stimulates apoptosis (61). We then performed western blot analysis to further evaluate the effect of m.7516delA mutation on apoptosis by measuring the levels of cytochrome *c* and three apoptosis-activated proteins [cleaved caspases 9 and 3 and cleaved poly(ADP-ribose) polymerase (Parp)] in mutant and control cybrids (61). As shown in Figure 9C, the marked increasing levels of cytochrome *c* and three apoptosis-activated proteins were observed in the mutant cell lines. As shown in Figure 9D, the average levels of cytochrome *c*, Caspase 9, Caspase 3 and Parp in three mutant cell lines were 146.3%, 119.2%, 230.1% and 214.2% of the mean values measured in three control cell lines, respectively ($P < 0.01$).

DISCUSSION

In this study, we demonstrated the profound impact of deafness-associated m.7516delA mutation on mitochondrial RNA processing contributing to the pathological process of deafness. This mutation was only present in the matrilineal relatives of the Chinese family with maternal inheritance of deafness. In fact, the m.7516delA mutation located at 3 bp (7515AAA/TTT7517) spacers between $tRNA^{Asp}$ and $tRNA^{Ser(UCN)}$ (4,27). The 3 bp (AAA/TTT) spacers are the 5′ end processing sites of $tRNA^{Asp}$ from the H-strand transcripts and $tRNA^{Ser(UCN)}$ from the L-strand transcripts, catalyzed by RNase P (6,7,10). Therefore, the primary defects arising from the deletion of adenine at position 7516 were the aberrant 5′ end processing of $tRNA^{Asp}$ from H-strand transcripts and the $tRNA^{Ser(UCN)}$ from the L-strand transcripts. These tRNA processing defects were evidenced by reduced efficiencies of the 5′ end processing of $tRNA^{Asp}$ and $tRNA^{Ser(UCN)}$ precursors carrying the m.7516delA mutation, catalyzed by RNase P, *in vitro* processing experiment and supported by decreased levels of $tRNA^{Asp}$ and $tRNA^{Ser(UCN)}$ observed in the cells bearing the m.7516delA mutation. However, there were remarkable differences in RNA processing defects arising from the m.7516delA mutation between the L-strand and H-strand polycistronic transcripts. On the H-strand transcript, the aberrant $tRNA^{Asp}$ 5′ end processing caused by the m.7516delA mutation specifically altered the processing of downstream COX2 precursors, evidenced by lower levels of COX2 mRNA and the accumulation of longer and uncleaved precursors [72 nt (7446–7517) + $tRNA^{Asp}$ + COX2] in the mutant cybrids, as compared with those in control cybrids. These reflected the complexity of the RNA processing of mitochondrial polycistronic transcripts, in addition to the tRNA punctuation model (7). In contrast, the m.7516delA mutation did not affect the processing of other 13 tRNAs includ-

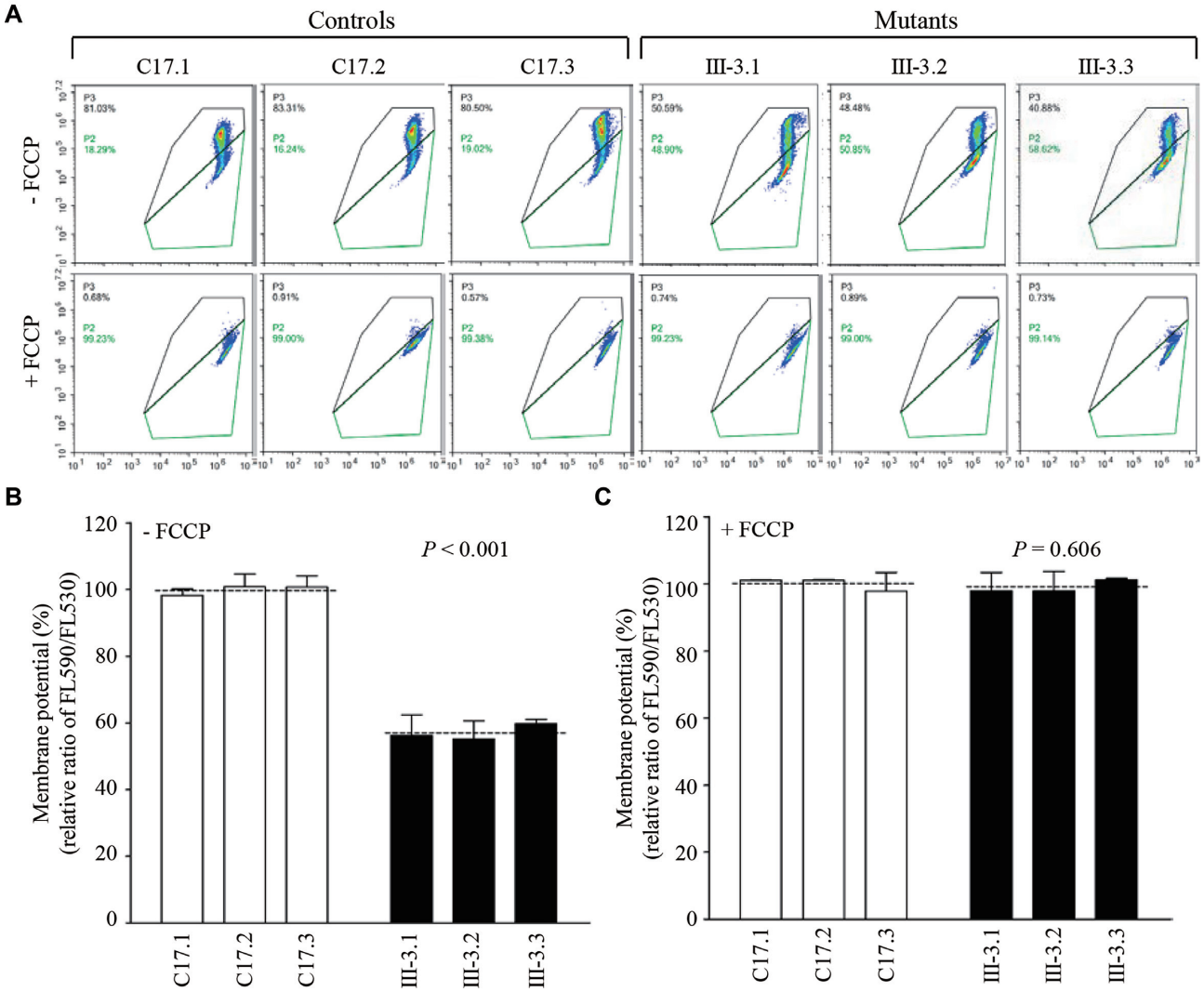

Figure 7. Mitochondrial membrane potential analysis. The mitochondrial membrane potential ($\Delta\Psi_m$) was measured in mutant and control cell lines using a fluorescence probe JC-10 assay system. The ratios of fluorescence intensities Ex/Em = 490/590 and 490/530 nm (FL590/FL530) were recorded to delineate the $\Delta\Psi_m$ level of each sample. The relative ratios of FL590/FL530 geometric mean between mutant and control cell lines were calculated to reflect the level of $\Delta\Psi_m$. (**A**) Represented flow cytometry images of mutant and control cell lines without and with 10 μM FCCP. Relative ratio of JC-10 fluorescence intensities at Ex/Em = 490/525 and 490/590 nm in the absence (**B**) and presence (**C**) of 10 μM FCCP in three control cell lines and three mutant cell lines. The average of three determinations for each cell line is shown. Graph details and symbols are explained in the legend to Figure 3.

ing $tRNA^{Leu(UUR)}$, $tRNA^{Gly}$, 11 mRNAs such as ND1 and COX1, 12S rRNA and 16S rRNA, which are co-transcribed from the L-strand mtDNA (6–8). These observations were in contrast with the observations that the aberrant $tRNA^{Met}$ 5′ end processing caused by the m.4401A>G mutation did not affect the processing of COX2 (26). On the L-strand transcript, the m.7516delA mutation impaired the processing of $tRNA^{Ser(UCN)}$ and downstream $tRNA^{Ala}$, $tRNA^{Asn}$, $tRNA^{Cys}$, $tRNA^{Tyr}$ and $tRNA^{Gln}$ but did not affect the processing of upstream $tRNA^{Glu}$, $tRNA^{Pro}$ and ND6 mRNA. These were evidenced by decreased levels of $tRNA^{Ser(UCN)}$, $tRNA^{Ala}$, $tRNA^{Asn}$, $tRNA^{Cys}$, $tRNA^{Gln}$ and $tRNA^{Tyr}$ in the mutant cybrids harboring the m.7516delA mutation. In contrast, the m.4401A>G mutation not only altered the 3′ end processing of all eight tRNA precursors but also had effects on the ND6 expression in the L-strand transcripts (26), while the $tRNA^{Ile}$ 4263A>G and $tRNA^{Ala}$ 5655A>G mutations only altered the 5′ end processing of $tRNA^{Ile}$ and $tRNA^{Ala}$, respectively (24,25). The asymmetrical effects of m.7516delA mutation on the processing of RNAs in the H-strand and L-strand polycistronic transcripts highlighted the different processing mechanisms of mitochondrial H-strand and L-strand polycistronic transcripts. These data are strong evidence that defects in the mitochondrial tRNA processing are the primary contributors to the pathological process of deafness.

The m.7516delA mutation-induced failure in metabolisms of seven tRNAs and COX2 mRNAs likely affected the efficiencies and fidelity of mitochondrial translation, especially impaired synthesis of those polypeptides with high codon usages of these tRNAs. Here, the mutant cybrids displayed variable decreases (an average decrease

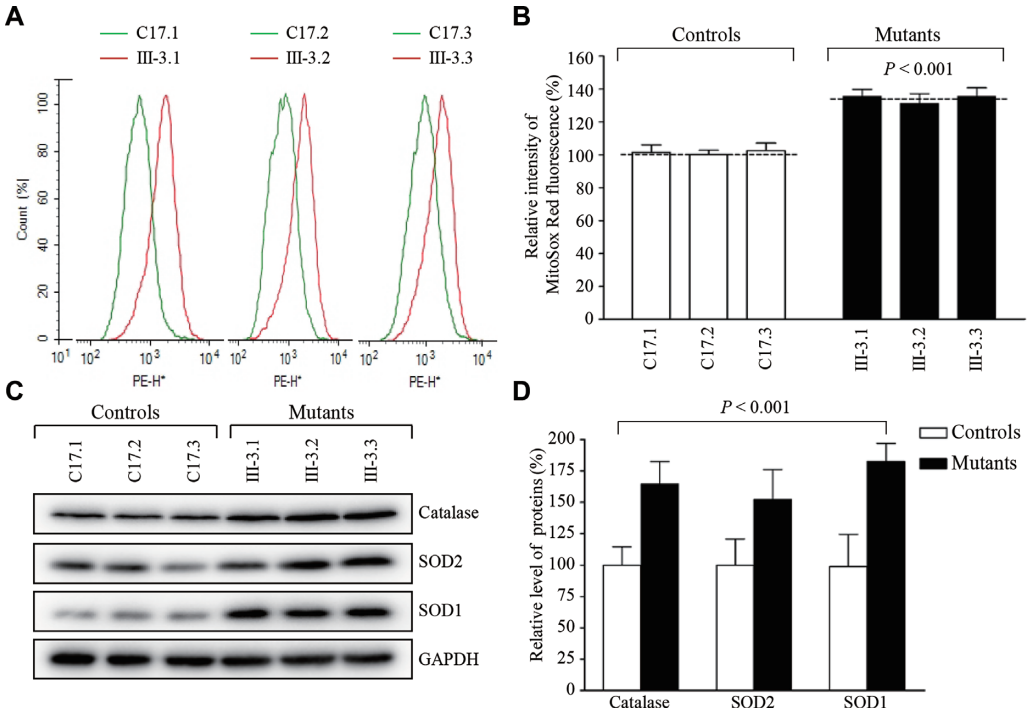

Figure 8. Measurement of mitochondrial ROS production. The levels of ROS generation by mitochondria in living cells from mutant and control cell lines were analyzed by the Novocyte flow cytometer (ACEA Biosciences) system using MitoSOX-Red Mitochondrial Superoxide Indicator. (**A**) Flow cytometry histogram showing MitoSOX-Red fluorescence of three control cybrids (green) and three mutant cybrids (red). (**B**) Relative ratios of MitoSOX-Red fluorescence intensity. (**C**) Western blot analysis of antioxidative enzymes SOD1, SOD2 and catalase in various cell lines with GAPDH as a loading control. (**D**) Quantification of SOD1, SOD2 and catalase. Average relative values of SOD1, SOD2 and catalase were normalized to the average values of GAPDH in various cell lines. The values for the latter are expressed as percentages of the average values for the control cell lines. The average of three independent determinations for each cell lines is shown. Graph details and symbols are explained in the legend to Figure 3.

of ∼28.4%) in nine mtDNA-encoded polypeptides, comparable effects seen in cells bearing the m.4263A>G, m.4401A>G or m.5655A>G mutation (24–26). Notably, mutant cybrids carrying the m.7516delA mutation exhibited marked reductions (44–65%) in the levels of five polypeptides (ND4, ND5, CO1, CO2 and CO3) harboring higher numbers of these codons. Strikingly, the reduction of CO2 resulted from both shortage of seven tRNAs and lower levels of COX2 mRNA, caused by the m.7516delA mutation. However, the levels of CYTB with higher numbers or proportions of these codons in mutant cybrids were comparable with those in control cybrids, while mutant cybrids displayed minor reductions (4%) in the levels of ATP8 carrying relative lower numbers of codons and even mild increases (∼5%) in the levels of ND1 and ND6 bearing extremely lower numbers of codons. Thus, no significant correlation of the reduced levels of these polypeptides in mutant cybrids with the numbers or proportions of overall aspartic acid, serine (UCN), alanine, tyrosine, asparagine, cysteine and glutamin codons (Supplementary Table S3), was in contrast with to what was previously shown in cells carrying the $tRNA^{Lys}$ 8344A>G and $tRNA^{Ser(UCN)}$ 7445A>G mutations (13,62). Alternatively, these translational defects may be due to the m.7516delA-induced mitoribosome stalling during the translation process, as in the case of $tRNA^{Leu(UUR)}$ 3243A>G mutation (63). Furthermore, the levels of four subunits of OXPHOS complexes (NDUFB8, SDHB, UQCRC2 and ATP5A) encoded by nuclear genes were not changed in the mutant cybrids bearing the m.7516delA mutation, indicating no effect of the m.7516delA mutation on the stability of OXPHOS complexes. However, the aberrant synthesis of mtDNA-encoded proteins produced the proteostasis stress, such as elevating the protein degradation in mitochondria, was evidenced by the increased levels of Lonp1, Afg3l2 and Clpp in the mutant cell lines (54–56,64).

The alterations in mitochondrial translation and induced proteostasis stress led to the deficient oxidative phosphorylation, increased ROS production and subsequent failure of cellular energetic processes (9,65–67). In particular, the impaired synthesis of ND4, ND5, CO1, CO2 and CO3 resulted in the decreased activities of complexes I and IV. Furthermore, the impairment of mitochondrial translation yielded the reduced rates in the basic OCR, ATP-linked OCR, proton leak OCR, reserve capacity OCR and maximal OCR in the mutant cell lines. The resultant respiratory deficiencies diminished mitochondrial ATP production and membrane potential and increased the ROS production. Alterations in OXPHOS and mitochondrial membrane potential as well as elevation of mitochondrial ROS production induced mitochondria-dependent apoptotic death (31,42,68,69). In this study, cybrids harboring the m.7516delA mutation displayed heightened vulnerability to apoptotic induction. These were evidenced by the elevated release of cytochrome *c* into cytosol and increased levels of caspases 3, 7 and 9 and PARP observed in cell

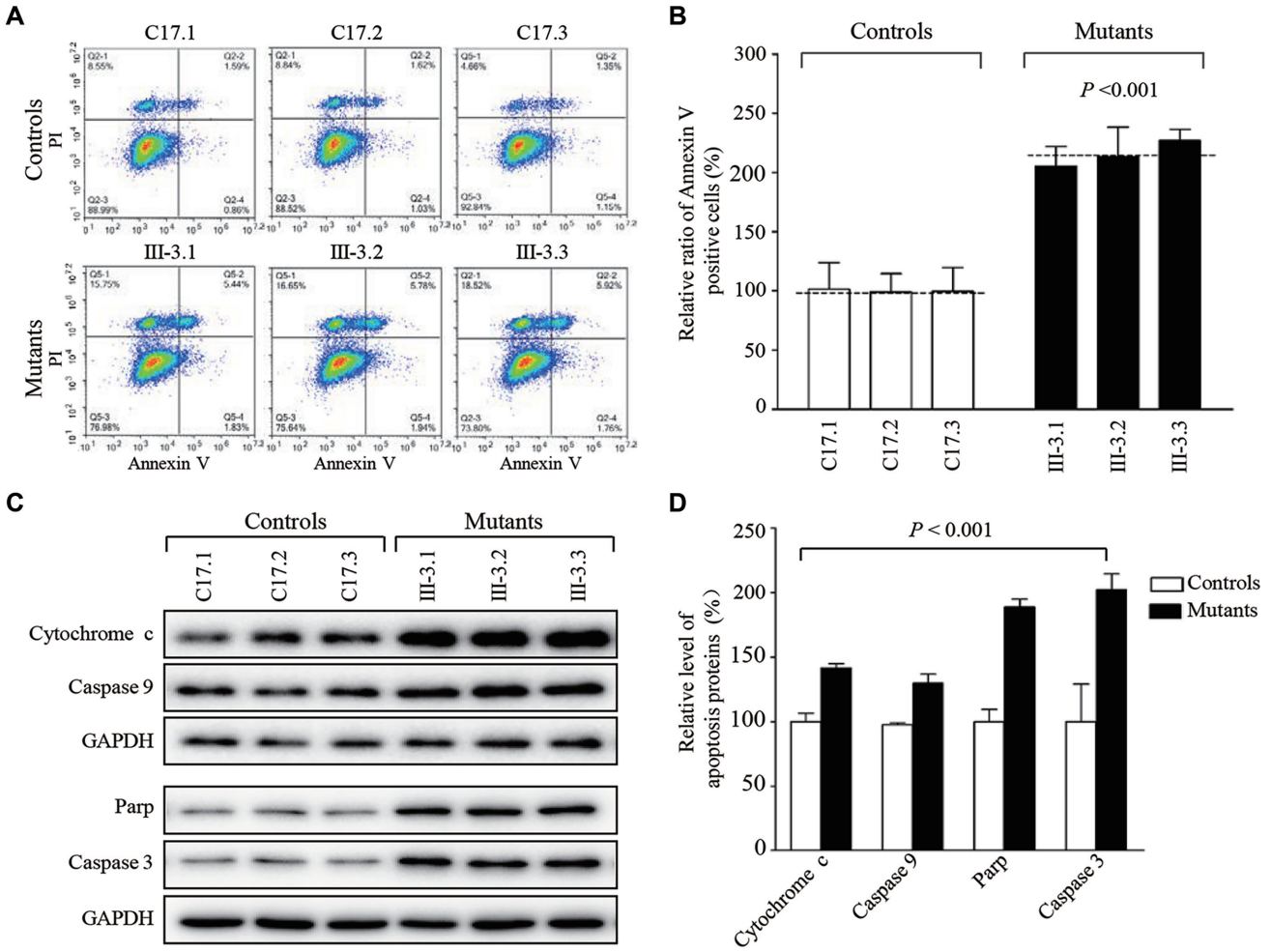

Figure 9. Analysis of apoptosis. (**A**) Annexin V/PI apoptosis assay by flow cytometry. Cells were harvested and stained with Annexin V and 1 μl of PI. Flow cytometric plots show cells in the live, early apoptosis and late apoptosis stages. Apoptosis rate increased in mutant cells compared with control cells. (**B**) Relative Annexin V-positive cells from various cell lines. Three independent determinations were done in each cell line. (**C**) Western blot analysis of cytochrome C and three apoptosis-activated proteins. Twenty micrograms of total proteins from various cell lines were electrophoresed, electroblotted and hybridized with cleaved Caspase 9, cleaved Parp and cleaved Caspase 3 antibodies and with GAPDH as a loading control. (**D**) Quantification of four proteins associated with apoptosis. Three independent determinations were done in each cell line. Graph details and symbols are explained in the legend to Figure 3.

lines carrying the m.7516delA mutation, as compared to control cybrids. These data suggested that mitochondrial dysfunction caused by the m.7516delA mutation promoted the apoptosis on the hair cells and neurons in the cochlea, because cochlear functions depended on a very high rate of ATP production (70,71). However, the incomplete penetrance of deafness and relatively mild biochemical defects indicated that the m.7516delA mutation might not be sufficient to produce the deafness phenotype. The nuclear modifier genes may contribute to the development of hearing-specific phenotype in these subjects carrying the mtDNA mutation(s) (72). Alternatively, the tissue-specific effects may arise from differential expression of tRNA genes (73,74) or variable activations of the integrated stress response pathway, metabolic changes and the ability of certain tissues to respond to impaired mitochondrial translation (75).

In summary, we demonstrated the profound impact of deafness-associated m.7516delA mutation on mitochondrial RNA processing contributing to the pathological process of deafness. The primary defects in the m.7516delA mutation were the aberrant 5′ end processing of $tRNA^{Asp}$ and $tRNA^{Ser(UCN)}$ precursors. The m.7516delA mutation caused the low levels of $tRNA^{Asp}$ and COX2 mRNA and the accumulation of longer and uncleaved precursors of COX2 from the H-strand transcript, and the significant decreases in the levels of $tRNA^{Ser(UCN)}$ and downstream five tRNAs from the L-strand transcript. These data demonstrated the asymmetrical effect of m.7516delA mutation on the expression of RNA from H-strand and L-strand polycistronic transcripts. These RNA metabolic defects resulted in the impairment of mitochondrial translation, proteostasis stress, respiratory deficiency, diminished membrane potential, increased production of reactive oxygen species and promoted apoptosis. Our findings provide new insights into the pathophysiology of maternal transmission of deafness arising from mitochondrial tRNA processing defects.

SUPPLEMENTARY DATA

Supplementary Data are available at NAR Online.

ACKNOWLEDGEMENTS

We are grateful to patients and their family members for their participation.

FUNDING

Ministry of Science and Technology of Zhejiang Province [2018C03026]; National Key Research and Devlopment Program of China [2018YFC1004802]; National Basic Research Priorities Program of China [2014CB541704 to M.-X.G.]; National Natural Science Foundation of China [82030028 to M.-X.G, 81670932 to H.W.]; The Key Projects of Shangdong Provincial Programs for Research and Development [2017CXGC1213 to H.W.].

Conflict of interest statement. None declared.

REFERENCE

1. Suzuki,T., Nagao,A. and Suzuki,T. (2011) Human mitochondrial tRNAs: biogenesis, function, structural aspects, and diseases. *Annu. Rev. Genet.*, **45**, 299–329.
2. Hällberg,B.M. and Larsson,N.G. (2014) Making proteins in the powerhouse. *Cell Metab.*, **20**, 226–240.
3. D'Souza,A.R. and Minczuk,M. (2018) Mitochondrial transcription and translation: overview. *Essays Biochem.*, **62**, 309–320.
4. Anderson,S., Bankier,A.T., Barrell,B.G., de Bruijn,M.H., Coulson,A.R., Drouin,J., Eperon,I.C., Nierlich,D.P., Roe,B.A., Sanger,F. *et al.* (1981) Sequence and organization of the human mitochondrial genome. *Nature*, **290**, 457–465.
5. Attardi,G. and Schatz,G. (1988) Biogenesis of mitochondria. *Annu. Rev. Cell Biol.*, **4**, 289–333.
6. Montoya,J., Gaines,G.L. and Attardi,G. (1983) The pattern of transcription of the human mitochondrial rRNA genes reveals two overlapping transcription units. *Cell*, **34**, 151–159.
7. Ojala,D., Montoya,J. and Attardi,G. (1981) tRNA punctuation model of RNA processing in human mitochondria. *Nature*, **290**, 470–474.
8. Scarpulla,R.C. (2008) Transcriptional paradigms in mammalian mitochondrial biogenesis and function. *Physiol. Rev.*, **88**, 611–638
9. Wallace,D.C. (2005) A mitochondrial paradigm of metabolic and degenerative diseases, aging, and cancer: a dawn for evolutionary medicine. *Annu. Rev. Genet.*, **39**, 359–407.
10. Mercer,T.R., Neph,S., Dinger,M.E., Crawford,J., Smith,M.A., Shearwood,A.M., Haugen,E., Bracken,C.P., Rackham,O., Stamatoyannopoulo,J.A. *et al.* (2011) The human mitochondrial transcriptome. *Cell*, **146**, 645–658.
11. Fisher,R.P., Topper,J.N. and Clayton,D.A. (1987) Promoter selection in human mitochondria involves binding of a transcription factor to orientation-independent upstream regulatory elements. *Cell*, **50**, 247–258.
12. Sanchez,M.I., Mercer,T.R., Davies,S.M., Shearwood,A.M., Nygard,K.K., Richman,T.R., Mattick,J.S., Rackham,O. and Filipovska,A. (2011) RNA processing in human mitochondria. *Cell Cycle*, **10**, 2904–2916.
13. Guan,M.X., Enriquez,J.A., Fischel-Ghodsian,N., Puranam,R.S., Lin,C.P., Maw,M.A. and Attardi,G. (1998) The deafness-associated mitochondrial DNA mutation at position 7445, which affects $tRNA^{Ser(UCN)}$ precursor processing, has long-range effects on NADH dehydrogenase subunit ND6 gene expression. *Mol. Cell. Biol.*, **18**, 5868–5879.
14. Brzezniak,L.K., Bijata,M., Szczesny,R.J. and Stepien,P.P. (2011) Involvement of human ELAC2 gene product in 3′ end processing of mitochondrial tRNAs. *RNA Biol.*, **8**, 616–626.
15. Holzmann,J., Frank,P., Loffler,E., Bennett,K.L., Gerner,C. and Rossmanith,W. (2008) RNase P without RNA: identification and functional reconstitution of the human mitochondrial tRNA processing enzyme. *Cell*, **135**, 462–474.
16. Reinhard,L., Sridhara,S. and Hallberg,B.M. (2017) The MRPP1/MRPP2 complex is a tRNA-maturation platform in human mitochondria. *Nucleic Acids Res.*, **45**, 12469–12480.
17. Temperley,R.J., Wydro,M., Lightowlers,R.N. and Chrzanowska-Lightowlers,Z.M. (2010) Human mitochondrial mRNAs—like members of all families, similar but different. *Biochim. Biophys. Acta*, **1797**, 1081–1085.
18. Van Haute,L., Pearce,S.F., Powell,C.A., D'Souza,A.R., Nicholls,T.J. and Minczuk,M. (2015) Mitochondrial transcript maturation and its disorders. *J. Inherit. Metab. Dis.*, **38**, 655–680.
19. Yan,H., Zareen,N. and Levinger,L. (2006) Naturally occurring mutations in human mitochondrial pre-$tRNA^{Ser(UCN)}$ can affect the transfer ribonuclease Z cleavage site, processing kinetics, and substrate secondary structure. *J. Biol. Chem.*, **281**, 3926–3935.
20. Levinger,L., Giegé,R. and Florentz,C. (2003) Pathology-related substitutions in human mitochondrial $tRNA^{Ile}$ reduce precursor 3′ end processing efficiency *in vitro*. *Nucleic Acids Res.*, **31**, 1904–1192.
21. Levinger,L. and Serjanov,D. (2012) Pathogenesis-related mutations in the T-loops of human mitochondrial tRNAs affect 3′ end processing and tRNA structure. *RNA Biol.*, **9**, 283–291.
22. Xue,L., Wang,M., Li,H., Wang,H., Jiang,F., Hou,L., Geng,J., Lin,Z., Peng,Y., Zhou,H. *et al.* (2016) Mitochondrial tRNA mutations in 2070 Chinese Han subjects with hypertension. *Mitochondrion*, **30**, 208–221.
23. Li,R., Liu,Y., Li,Z., Yang,L., Wang,S. and Guan,M.X. (2009) Failures in mitochondrial $tRNA^{Met}$ and $tRNA^{Gln}$ metabolism caused by the novel 4401A>G mutation are involved in essential hypertension in a Han Chinese Family. *Hypertension*, **54**, 329–337.
24. Wang,S., Li,R., Fettermann,A., Li,Z., Qian,Y., Liu,Y., Wang,X., Zhou,A., Mo,J.Q., Yang,L. *et al.* (2011) Maternally inherited essential hypertension is associated with the novel 4263A>G mutation in the mitochondrial $tRNA^{Ile}$ gene in a large Han Chinese family. *Circ. Res.*, **108**, 862–870.
25. Jiang,P., Wang,M., Xue,L., Xiao,Y., Yu,J., Wang,H., Yao,J., Liu,H., Peng,Y., Liu,H. *et al.* (2016) A hypertension-associated $tRNA^{Ala}$ mutation alters tRNA metabolism and mitochondrial function. *Mol. Cell. Biol.*, **36**, 1920–1930.
26. Zhao,X., Cui,L., Xiao,Y., Mao,Q., Aishanjiang,M., Kong,W., Liu,Y., Chen,H., Hong,F., Jia,Z., Wang,M., Jiang,P. and Guan,M.X. (2019) Hypertension-associated mitochondrial DNA 4401A>G mutation caused the aberrant processing of $tRNA^{Met}$, all 8 tRNAs and ND6 mRNA in the light-strand transcript. *Nucleic Acids Res.*, **47**, 10340–10356.
27. Zheng,J., Bai,X., Xiao,Y., Ji,Y., Meng,F., Aishanjiang,M., Gao,Y., Wang,H., Fu,Y. and Guan,M.X. (2020) Mitochondrial tRNA mutations in 887 Chinese subjects with hearing loss. *Mitochondrion*, **52**, 163–172.
28. Florentz,C., Sohm,B., Tryoen-Toth,P., Putz,J. and Sissler,M. (2003) Human mitochondrial tRNAs in health and disease. *Cell. Mol. Life Sci.*, **60**, 1356–1375.
29. King,M.P. and Attardi,G. (1989) Human cells lacking mtDNA: repopulation with exogenous mitochondria by complementation. *Science*, **246**, 500–503.
30. Gong,S., Peng,Y., Jiang,P., Wang,M., Fan,M., Wang,X., Zhou,H., Li,H., Yan,Q., Huang,T. *et al.* (2014) A deafness-associated $tRNA^{His}$ mutation alters the mitochondrial function, ROS production and membrane potential. *Nucleic Acids Res.*, **42**, 8039–8048.
31. Zhang,J., Ji,Y., Lu,Y., Fu,R., Xu,M., Liu,X. and Guan,M.X. (2018) Leber's hereditary optic neuropathy (LHON)-associated ND5 12338T>C mutation altered the assembly and function of complex I, apoptosis and mitophagy. *Hum. Mol. Genet.*, **27**, 1999–2011.
32. Guan,M.X., Fischel-Ghodsian,N. and Attardi,G. (2001) Nuclear background determines biochemical phenotype in the deafness-associated mitochondrial 12S rRNA mutation. *Hum. Mol. Genet.*, **10**, 573–580.
33. Zhao,H., Li,R., Wang,Q., Yan,Q., Deng,J.H., Han,D., Bai,Y., Young,W.Y. and Guan,M.X. (2004) Maternally inherited aminoglycoside-induced and nonsyndromic deafness is associated with the novel C1494T mutation in the mitochondrial 12S rRNA gene in a large Chinese family. *Am. J. Hum. Genet.*, **74**, 139–152.
34. Yan,X., Wang,X., Wang,Z., Sun,S., Chen,G., He,Y., Mo,J.Q., Li,R., Jiang,P., Lin,Q. *et al.* (2011) Maternally transmitted late-onset non-syndromic deafness is associated with the novel heteroplasmic

T12201C mutation in the mitochondrial $tRNA^{His}$ gene. *J. Med. Genet.*, **48**, 682–690.
35. Andrews,R.M., Kubacka,I., Chinnery,P.F., Lightowlers,R.N., Turnbull,D.M. and Howell,N. (1999) Reanalysis and revision of the Cambridge reference sequence for human mitochondrial DNA. *Nat. Genet.*, **23**, 147.
36. Rieder,M.J., Taylor,S.L., Tobe,V.O. and Nickerson,D.A. (1998) Automating the identification of DNA variations using quality-based fluorescence re-sequencing: analysis of the human mitochondrial genome. *Nucleic Acids Res.*, **26**, 967–973.
37. Miller,G. and Lipman,M. (1973) Release of infectious Epstein–Barr virus by transformed marmoset leukocytes. *Proc. Natl Acad. Sci. U.S.A.*, **70**, 190–194.
38. Zhang,J., Liu,X., Liang,X., Lu,Y., Zhu,L., Fu,R., Ji,Y., Fan,W., Chen,J., Lin,B. *et al.* (2017) A novel ADOA-associated OPA1 mutation alters the mitochondrial function, membrane potential, ROS production and apoptosis. *Sci. Rep.*, **7**, 5704.
39. King,M.P. and Attardi,G. (1993) Post-transcriptional regulation of the steady-state levels of mitochondrial tRNAs in HeLa cells. *J. Biol. Chem.*, **268**, 10228–10237.
40. Zhou,M., Xue,L., Chen,Y., Li,H., He,Q., Wang,B., Meng,F., Wang,M. and Guan,M.X. (2018) A hypertension-associated mitochondrial DNA mutation introduces an m^1G37 modification into $tRNA^{Met}$, altering its structure and function. *J. Biol. Chem.*, **293**, 1425–1438.
41. Jiang,P., Jin,X., Peng,Y., Wang,M., Liu,H., Liu,X., Zhang,Z., Ji,Y., Zhang,J., Liang,M. *et al.* (2016) The exome sequencing identified the mutation in YARS2 encoding the mitochondrial tyrosyl-tRNA synthetase as a nuclear modifier for the phenotypic manifestation of Leber's hereditary optic neuropathy-associated mitochondrial DNA mutation. *Hum. Mol. Genet.*, **25**, 584–596.
42. Jia,Z., Zhang,Y., Li,Q., Ye,Z., Liu,Y., Fu,C., Cang,X., Wang,M. and Guan,M.X. (2019) A coronary artery disease-associated $tRNA^{Thr}$ mutation altered mitochondrial function, apoptosis and angiogenesis. *Nucleic Acids Res.*, **47**, 2056–2074.
43. Wang,M., Peng,Y., Zheng,J., Zheng,B., Jin,X., Liu,H., Wang,Y., Tang,X., Huang,T., Jiang,P. *et al.* (2016) A deafness-associated $tRNA^{Asp}$ mutation alters the m^1G37 modification, aminoacylation and stability of $tRNA^{Asp}$ and mitochondrial function. *Nucleic Acids Res.*, **44**, 10974–10985.
44. Li,X., Fischel-Ghodsian,N., Schwartz,F., Yan,Q., Friedman,R.A. and Guan,M.X. (2004) Biochemical characterization of the mitochondrial $tRNA^{Ser(UCN)}$ T7511C mutation associated with nonsyndromic deafness. *Nucleic Acids Res.*, **32**, 867–877.
45. Gong,S., Wang,X., Meng,F., Cui,L., Yi,Q., Zhao,Q., Cang,X., Cai,Z., Mo,J.Q., Liang,Y. *et al.* (2020) Overexpression of mitochondrial histidyl-tRNA synthetase restores mitochondrial dysfunction caused by a deafness-associated $tRNA^{His}$ mutation. *J. Biol. Chem.*, **295**, 940–954.
46. Meng,F., He,Z., Tang,X., Zheng,J., Jin,X., Zhu,Y., Ren,X., Zhou,M., Wang,M., Gong,S. *et al.* (2018) Contribution of the $tRNA^{Ile}$ 4317A>G mutation to the phenotypic manifestation of the deafness-associated mitochondrial 12S rRNA 1555A>G mutation. *J. Biol. Chem.*, **293**, 3321–3334.
47. Dranka,B.P., Benavides,G.A., Diers,A.R., Giordano,S., Zelickson,B.R., Reily,C., Zou,L., Chatham,J.C., Hill,B.G., Zhang,J. *et al.* (2011) Assessing bioenergetic function in response to oxidative stress by metabolic profiling. *Free Radic. Biol. Med.*, **51**, 1621–1635.
48. Li,Y., D'Aurelio,M., Deng,J. H., Park,J. S., Manfredi,G., Hu,P., Lu,J. and Bai,Y. (2007) An assembled complex IV maintains the stability and activity of complex I in mammalian mitochondria. *J. Biol. Chem.*, **282**, 17557–17562.
49. Thorburn,D.R., Chow,C.W. and Kirby,D.M. (2004) Respiratory chain enzyme analysis in muscle and liver. *Mitochondrion*, **4**, 363–375.
50. Reers,M., Smiley,S.T., Mottola-Hartshorn,C., Chen,A., Lin,M. and Chen,L.B. (1995) Mitochondrial membrane potential monitored by JC-1 dye. *Methods Enzymol.*, **260**, 406–417.
51. Mahfouz,R., Sharma,R., Lackner,J., Aziz,N. and Agarwal,A. (2009) Evaluation of chemiluminescence and flow cytometry as tools in assessing production of hydrogen peroxide and superoxide anion in human spermatozoa. *Fertil. Steril.*, **92**, 819–827.
52. Yu,J., Zheng,J., Zhao,X., Liu,J., Mao,Z., Ling,Y., Chen,D., Chen,C., Hui,L., Cui,L. *et al.* (2014) Aminoglycoside stress together with the 12S rRNA 1494C>T mutation leads to mitophagy. *PLoS One*, **9**, e114650.
53. Ji,Y., Zhang,J., Lu,Y., Yi,Q., Chen,M., Xie,S., Mao,X., Xiao,Y., Meng,F. *et al.* (2020) Complex I mutations synergize to worsen the phenotypic expression of Leber's hereditary optic neuropathy. *J. Biol. Chem.*, **295**, 13224–13238.
54. Li,Y., Liu,L., Zhu,Y. and Chen,Q. (2019) Mitochondria organize the cellular proteostatic response and promote cellular senescence. *Cell Stress*, **3**, 110–114.
55. Szczepanowska,K., Maiti,P., Kukat,A., Hofsetz,E., Nolte,H., Senft,K., Becker,C., Ruzzenente,B., Hornig-Do,H.T., Wibom,R. *et al.* (2016) CLPP coordinates mitoribosomal assembly through the regulation of ERAL1 levels. *EMBO J.*, **35**, 2566–2583.
56. Nolden,M., Ehses,S., Koppen,M., Bernacchia,A., Rugarli,E.I. and Langer,T. (2005) The m-AAA protease defective in hereditary spastic paraplegia controls ribosome assembly in mitochondria. *Cell*, **123**, 277–289.
57. Scheffler,I.E. (2015) Mitochondrial disease associated with complex I (NADH-CoQ oxidoreductase) deficiency. *J. Inherit. Metab. Dis.*, **38**, 405–415.
58. Thorburn,D.R., Chow,C.W. and Kirby,D.M. (2004) Respiratory chain enzyme analysis in muscle and liver. *Mitochondrion*, **4**, 363–375.
59. Sena,L.A. and Chandel,N.S. (2012) Physiological roles of mitochondrial reactive oxygen species. *Mol. Cell*, **48**, 158–167.
60. Schieber,M. and Chandel,N.S. (2014) ROS function in redox signaling and oxidative stress. *Curr. Biol.*, **24**, R453–R462.
61. Taylor,R.C., Cullen,S.P. and Martin,S.J. (2008) Apoptosis: controlled demolition at the cellular level. *Nat. Rev. Mol. Cell. Biol.*, **9**, 231–241.
62. Enriquez,J.A., Chomyn,A. and Attardi,G. (1995) MtDNA mutation in MERRF syndrome causes defective aminoacylation of $tRNA^{Lys}$ and premature translation termination. *Nat. Genet.*, **10**, 47–55.
63. Chomyn,A., Enriquez,J.A., Micol,V., Fernandez-Silva,P. and Attardi,G. (2000) The mitochondrial myopathy, encephalopathy, lactic acidosis, and stroke-like episode syndrome-associated human mitochondrial $tRNA^{Leu(UUR)}$ mutation causes aminoacylation deficiency and concomitant reduced association of mRNA with ribosomes. *J. Biol. Chem.*, **275**, 19198–19209.
64. Chen,D., Zhang,Z., Chen,C., Yao,S., Yang,Q., Li,F., He,X., Ai,C., Wang,M. and Guan,M.X. (2019) Deletion of Gtpbp3 in zebrafish revealed the hypertrophic cardiomyopathy manifested by aberrant mitochondrial tRNA metabolism. *Nucleic Acids Res.*, **47**, 5341–5355.
65. Münch,C. and Harper,J.W. (2016) Mitochondrial unfolded protein response controls matrix pre-RNA processing and translation. *Nature*, **534**, 710–713.
66. Smeitink,J., van den Heuvel,L. and DiMauro,S. (2001) The genetics and pathology of oxidative phosphorylation. *Nat. Rev. Genet.*, **2**, 342–352.
67. Meng,F., Cang,X., Peng,Y., Li,R., Zhang,Z., Li,F., Fan,Q., Guan,A.S., Fischel-Ghosian,N., Zhao,X. *et al.* (2017) Biochemical evidence for a nuclear modifier allele (A10S) in TRMU (methylaminomethyl-2-thiouridylate-methyltransferase) related to mitochondrial tRNA modification in the phenotypic manifestation of deafness-associated 12S rRNA mutation. *J. Biol. Chem.*, **292**, 2881–2892.
68. Kawamata,H. and Manfredi,G. (2017) Proteinopathies and OXPHOS dysfunction in neurodegenerative diseases. *J. Cell Biol.*, **216**, 3917–3929.
69. Kang,Y., Anderson,A.J., Jackson,T.D., Palmer,C.S., De Souza,D.P., Fujihara,K.M., Stait,T., Frazier,A.E., Clemons,N.J., Tull,D. *et al.* (2019). Function of hTim8a in complex IV assembly in neuronal cells provides insight into pathomechanism underlying Mohr–Tranebjærg syndrome. *eLife*, **8**, e48828.
70. Ceriani,F., Pozzan,T. and Mammano,F. (2016) Critical role of ATP-induced ATP release for Ca^{2+} signaling in nonsensory cell networks of the developing cochlea. *Proc. Natl Acad. Sci. U.S.A.*, **113**, E7194–E7201.
71. Guan,M.X. (2004) Molecular pathogenetic mechanism of maternally inherited deafness. *Ann. N.Y. Acad. Sci.*, **1011**, 259–271.
72. Guan,M.X., Yan,Q., Li,X., Bykhovskaya,Y., Gallo-Teran,J., Hajek,P., Umeda,N., Zhao,H., Garrido,G., Mengesha,E. *et al.* (2006) Mutation in TRMU related to transfer RNA modification modulates the phenotypic expression of the deafness-associated mitochondrial 12S ribosomal RNA mutations. *Am. J. Hum. Genet.*, **79**, 291–302.

73. Torres,A.G., Reina,O., Stephan-Otto Attolini,C. and Ribas de Pouplana,L. (2019) Differential expression of human tRNA genes drives the abundance of tRNA-derived fragments. *Proc. Natl Acad. Sci. U.S.A.*, **116**, 8451–8456.
74. Dittmar,K.A., Goodenbour,J.M. and Pan,T. (2006) Tissue-specific differences in human transfer RNA expression. *PLoS Genet.*, **2**, e221.
75. Agnew,T., Goldsworthy,M., Aguilar,C., Morgan,A., Simon,M., Hilton,H., Esapa,C., Wu,Y., Cater,H., Bentley,L. *et al.* (2018) A Wars2 mutant mouse model displays OXPHOS deficiencies and activation of tissue-specific stress response pathways. *Cell Rep.*, **25**, 3315–3328.